ISPRS Journal of Photogrammetry and Remote Sensing 99 (2015) 70–83

Contents lists available at ScienceDirect

ISPRS Journal of Photogrammetry and Remote Sensing

journal homepage: www.elsevier.com/locate/isprsjprs

Estimation and analysis of gross primary production of soybean under various management practices and drought conditions

Pradeep Wagle [a], Xiangming Xiao [a,b,*], Andrew E. Suyker [c]

[a] Department of Microbiology and Plant Biology, Center for Spatial Analysis, University of Oklahoma, Norman, OK 73019, USA
[b] Institute of Biodiversity Science, Fudan University, Shanghai, China
[c] School of Natural Resource, University of Nebraska–Lincoln, Lincoln, NE 68583, USA

ARTICLE INFO

Article history:
Received 18 August 2014
Received in revised form 25 October 2014
Accepted 27 October 2014

Keywords:
Gross primary production
Light use efficiency
Remote sensing
Vapor pressure deficit
Vegetation indices
Vegetation photosynthesis model

ABSTRACT

Gross primary production (GPP) of croplands may be used to quantify crop productivity and evaluate a range of management practices. Eddy flux data from three soybean (*Glycine max* L.) fields under different management practices (no-till vs. till; rainfed vs. irrigated) and Moderate Resolution Imaging Spectroradiometer (MODIS) derived vegetation indices (VIs) were used to test the capabilities of remotely sensed VIs and soybean phenology to estimate the seasonal dynamics of carbon fluxes. The modeled GPP (GPP_{VPM}) using vegetation photosynthesis model (VPM) was compared with the GPP (GPP_{EC}) estimated from eddy covariance measurements. The VIs tracked soybean phenology well and delineated the growing season length (GSL), which was closely related to carbon uptake period (CUP, $R^2 = 0.84$), seasonal sums of net ecosystem CO_2 exchange (NEE, $R^2 = 0.78$), and GPP_{EC} ($R^2 = 0.54$). Land surface water index (LSWI) tracked drought-impacted vegetation well, as the LSWI values were positive during non-drought periods and negative during severe droughts within the soybean growing season. On a seasonal scale, NEE of the soybean sites ranged from −37 to −264 g C m^{-2}. The result suggests that rainfed soybean fields needed about 450–500 mm of well-distributed seasonal rainfall to maximize the net carbon sink. During non-drought conditions, VPM accurately estimated seasonal dynamics and interannual variation of GPP of soybean under different management practices. However, some large discrepancies between GPP_{VPM} and GPP_{EC} were observed under drought conditions as the VI did not reflect the corresponding decrease in GPP_{EC}. Diurnal GPP_{EC} dynamics showed a bimodal distribution with a pronounced midday depression at the period of higher water vapor pressure deficit (>1.2 kPa). A modified W_{scalar} based on LSWI to account for the water stress in VPM helped quantify the reduction in GPP during severe drought and the model's performance improved substantially. In conclusion, this study demonstrates the potential of integrating vegetation activity through satellite remote sensing with ground-based flux and climate data for a better understanding and upscaling of carbon fluxes of soybean croplands.

1. Introduction

As atmospheric CO_2 concentration is rising due to anthropogenic activities, there is a growing interest for a better understanding of the dynamics of CO_2 fluxes. Over the last decade, a large number (>600) of eddy flux tower sites are established to determine net ecosystem CO_2 exchange [NEE, the balance between gross primary production (GPP) and ecosystem respiration (ER)] between terrestrial ecosystems and the atmosphere (Baldocchi et al., 2001). The NEE studies are used to assess the carbon uptake potential of ecosystems and GPP is estimated from NEE data (Falge et al., 2002). The GPP is used to quantify crop productivity, determine better management practices (Baker and Griffis, 2005), and understand temporal differences in productivity (Falge et al., 2002). In addition, CO_2 fluxes from terrestrial ecosystems are important to monitor atmospheric CO_2 concentrations (Baldocchi et al., 2001). In recent years, eddy flux data are the primary source of data to support model development and satellite remote sensing (Mahadevan et al., 2008; Running et al., 1999a; Stockli et al., 2008; Williams et al., 2009). The images from the Moderate Resolution Imaging Spectroradiometer (MODIS) sensor are used to estimate

* Corresponding author at: Department of Microbiology and Plant Biology, University of Oklahoma, 101 David L. Boren Blvd., Norman, OK 73019-5300, USA. Tel.: +1 (405) 325 8941 (Office), +1 (603) 560 5648 (Cell); fax: +1 (405) 325 3442.
E-mail address: xiangming.xiao@ou.edu (X. Xiao).
URL: http://www.eomf.ou.edu (X. Xiao).

http://dx.doi.org/10.1016/j.isprsjprs.2014.10.009
0924-2716/

GPP and net primary production (NPP) at 1 km spatial resolution (Running et al., 2004). These products provide valuable estimates of vegetation productivity, but it is important to validate these products with in-situ measurements. The NEE and GPP measurements from the eddy flux tower at the ecosystem-level provide opportunities for validating the MODIS NPP and GPP products (Turner et al., 2006).

While the majority of eddy flux tower sites are in natural and unmanaged ecosystems, a few eddy flux towers are established in managed agricultural ecosystems. More accurate information on GPP of croplands is of vital importance. In the U.S. North Central Region, agricultural row crops, small grain, and fallow land occupy 40% of the land area. Moreover, annual rotation of maize (*Zea mays* L.) and soybean (*Glycine max* L.) comprises 83% of the agricultural land devoted to row crops, small grain, and fallow. However, only a few short term NEE studies have been reported in soybean (Baker and Griffis, 2005; Gilmanov et al., 2014; Hollinger et al., 2005; Suyker et al., 2005). These studies have shown that soybean fields are near carbon neutral or even a small source of carbon on annual scales. There is still a lack of detailed information on carbon fluxes and the influence of major environmental factors on carbon fluxes of soybean fields under different management practices.

Maize/soybean rotations in the U.S. are either rainfed or irrigated agricultural ecosystems. Both conventional till and no-till management practices are common. It is known that carbon fluxes are subject to change with different management practices (Angers et al., 1997; Winjum et al., 1992). Accurate estimation of spatial patterns and temporal dynamics of GPP of soybean fields at larger spatial scales under different management practices is essential to improve our understanding of carbon dynamics of this globally important ecosystem. Thus, it is necessary to upscale site-specific flux observations beyond spatial limits of flux tower footprints. One upscaling approach is to use satellite remote sensing observations and climate data (Turner et al., 2003). Repetitive and systematic satellite remote sensing observations of vegetation dynamics and ecosystems allow us to characterize vegetation structure, and estimate GPP and NPP (Potter et al., 1993; Ruimy et al., 1994). A satellite-derived vegetation photosynthesis model (VPM) estimates GPP at daily to 8-day temporal scales and has been evaluated over several flux tower sites (Xiao et al., 2004a). Previous work has examined the simulated dynamics of GPP for the maize growing seasons from two of three study sites selected in this study (Kalfas et al., 2011). The GPP simulation of soybean systems under a range of hydrometeorological conditions is a focus of this study. Eddy covariance flux data and MODIS-derived vegetation indices (VIs) from three soybean fields were used to: (a) test the capabilities of remotely sensed VIs and soybean phenology to estimate seasonal carbon dynamics, and (b) explore the underlying mechanisms of environmental controls of CO_2 fluxes in soybean systems. In addition, we also compared the modeled GPP (GPP_{VPM}) using VPM and the MODIS GPP ($GPP_{MOD17A2}$) with GPP (GPP_{EC}) estimated from eddy covariance measurements.

2. Materials and methods

2.1. The study sites

2.1.1. The Rosemount site (US-Ro1)

This site (44.7143°N, 93.0898°W) is located at the University of Minnesota's Rosemount Research and Outreach Center, near St. Paul, Minnesota. Soil type is Waukegan silt loam (fine, mixed, mesic typic Hapludoll) with a surface layer of high organic carbon content (2.6% average) and variable thickness (0.3–2.0 m) underlain by coarse outwash sand and gravel. Prior to cultivation, the site was an upland dry prairie consisting mainly of C_4 and C_3 grasses. The harvesting of wheat (*Triticum aestivum* L.) began in 1879. Maize was consistently planted annually between 1998 and 2001. From 2002, it was changed to conventional-till management maize-soybean annual rotation field. This is a rain-fed agricultural system. Further information on site characteristics can be found in Griffis et al. (2007) and at the AmeriFlux website (http://ameriflux.ornl.gov/fullsiteinfo.php?sid=63).

2.1.2. The Mead irrigated rotation site (US-Ne2)

This site (41.1649°N, 96.4701°W) is located at the University of Nebraska Agricultural Research and Development Center, near Mead, Nebraska. The site is irrigated with a center-pivot system. This site had a 10-year history of maize-soybean rotation under no-till practice. A tillage operation (disking) was done just prior to the 2001 planting to homogenize the top 0.1 m of soil and to incorporate *P* and *K* fertilizers, as well as previously accumulated surface residues. Since this tillage operation, the site has been under no-till management. This site has deep, silty-clay loam soils. Details about this site can be found in Suyker et al. (2005) and at the AmeriFlux website (http://ameriflux.ornl.gov/fullsiteinfo.php?sid=73).

2.1.3. The Bondville site (US-Bo1)

This site (40.0062°N, 88.2904°W) is located in the Midwestern part of the United States, near Champaign, Illinois. The site has been in continuous no-till (since 1986) with alternating years of soybean and maize from 1996 to the present (maize in the odd years and soybean in the even years). This is a rain-fed agricultural system. Soil type is silt loam consisting three soil series (Dana, Flanagan, and Drummer). Detailed site descriptions and measurements can be found in Meyers and Hollinger (2004) and at the AmeriFlux website (http://ameriflux.ornl.gov/fullsiteinfo.php?sid=44).

2.2. CO_2 flux measurements

Flux densities of CO_2, sensible heat, latent heat, and momentum were measured using the eddy covariance technique. Site-specific climate data [air temperature, precipitation, photosynthetically active radiation (PAR), and soil water content] and Level-4 CO_2 flux data were acquired from the AmeriFlux website (http://ameriflux.ornl.gov/). The Level-4 data consists of CO_2 fluxes at half-hourly, daily, 8-day, and monthly time steps. The Marginal Distribution Sampling (MDS) method was used to fill gaps in data (Reichstein et al., 2005). Measured NEE data were partitioned to GPP and ER. Two years of data (2004 and 2006) for the Rosemount site (US-Ro1), two years of data (2002 and 2004) for the Mead irrigated rotation site (US-Ne2), and three years of data (2002, 2004, and 2006) for the Bondville site (US-Bo1) were used in this study. We determined the carbon uptake period (CUP) as the number of days when the ecosystem was a net sink of carbon (negative NEE). The CUP starts when vegetation is large enough to photosynthesize at higher rate than the rate of ER. The CUP ends after the senescence of vegetation when ER is higher than GPP. We summed NEE and GPP for the period of soybean growing season (May–October) to get seasonal sums.

2.3. Satellite-derived VIs data

The 8-day composite Land Surface Reflectance (MOD09A1) data from one MODIS pixel where the flux tower is geo-located were downloaded from the MODIS data portal at the Earth Observation and Modeling Facility (EOMF), University of Oklahoma (http://eomf.ou.edu/visualization/gmap/). Blue, green, red, near infrared (NIR), and shortwave infrared (SWIR) bands were used to derive VIs [enhanced vegetation index (EVI, Huete et al., 2002),

normalized difference vegetation index (NDVI, Tucker, 1979), and land surface water index (LSWI, Xiao et al., 2004a)] as follows:

$$\mathrm{NDVI} = \frac{\rho_{nir} - \rho_{red}}{\rho_{nir} + \rho_{red}} \quad (1)$$

$$\mathrm{EVI} = 2.5 \times \frac{\rho_{nir} - \rho_{red}}{\rho_{nir} + (6 \times \rho_{red} - 7.5 \times \rho_{blue}) + 1} \quad (2)$$

$$\mathrm{LSWI} = \frac{\rho_{nir} - \rho_{swir}}{\rho_{nir} + \rho_{swir}} \quad (3)$$

where ρ is surface reflectance in the wavelength band.

2.4. Growing season length based on VIs

The growing season length (GSL_{VI}) based on remotely sensed VIs was determined as the numbers of days the VIs (EVI and NDVI) were greater than given threshold values for each site–year. The threshold values were determined when NDVI and EVI stated to rise at the beginning of the crop growing season, and declined and approached to similar threshold values during harvesting or crop senescence. As both NDVI and EVI followed the same seasonal pattern there was no difference in the GSL as derived from NDVI or EVI. The threshold EVI values were about 0.20 and the NDVI values were about 0.30 across three sites. The EVI values were summed for the period of soybean growing season (May–October) to derive seasonal sums.

2.5. Vegetation photosynthesis model (VPM) and parameter estimations

The VPM estimates GPP as:

$$\mathrm{GPP_{VPM}} = \varepsilon_g \times \mathrm{FPAR}_{chl} \times \mathrm{PAR} \quad (4)$$

where ε_g is the light use efficiency [LUE, g C mol^{-1} photosynthetic photon flux density (PPFD)], $FPAR_{chl}$ is the fraction of PAR absorbed by chlorophyll, and PAR is the photosynthetically active radiation. The detailed description of VPM can be found in previous publications (Xiao et al., 2004a,b). Here only a brief review is presented.

In VPM, $FPAR_{chl}$ is estimated as a linear function of EVI, and the coefficient a is set to be 1.0 (Xiao et al., 2004a):

$$\mathrm{FPAR}_{chl} = a \times \mathrm{EVI} \quad (5)$$

Light use efficiency (ε_g) is affected by temperature and water stresses, and expressed as:

$$\varepsilon_g = \varepsilon_0 \times T_{scalar} \times W_{scalar} \quad (6)$$

where ε_0 is the apparent quantum yield or maximum light use efficiency (g C mol^{-1} PPFD), and T_{scalar} and W_{scalar} are scalars ranging from 0 to 1 that characterize the effects of temperature and water on GPP, respectively.

The ecosystem-level ε_0 values differ with vegetation types and can be determined from analysis of the NEE-PPFD relationship at eddy flux tower sites (Goulden et al., 1997). As the maximum value of ε_0 can be observed during peak growth, the ε_0 parameter was estimated using the Michaelis–Menten function (Eq. (7)) based on 7-day flux data at 30-min intervals during peak soybean growth.

$$\mathrm{NEE} = \frac{\varepsilon_0 \times \mathrm{GPP_{max}} \times \mathrm{PPFD}}{\varepsilon_0 \times \mathrm{PPFD} + \mathrm{GPP_{max}}} + \mathrm{ER} \quad (7)$$

where GPP_{max} is the maximum canopy CO_2 uptake rate ($\mu mol\ m^{-2}\ s^{-1}$) at light saturation and ER is the ecosystem respiration. The largest observed ε_0 value was approximately 0.07 mol CO_2 mol^{-1} PPFD (0.84 g C mol^{-1} PPFD) at the Bondville site (July 24–31, 2004) and the Rosemount site (August 8–15, 2004). The largest ε_0 value was approximately 0.053 mol CO_2 mol^{-1} PPFD (0.64 g C mol^{-1} PPFD) at the Mead site (July 24–31, 2004). Gilmanov et al. (2014) also reported a similar value of maximum ε_0 (0.068 mol CO_2 mol^{-1} PPFD) for soybean at the Rosemount site. To avoid circularity in the modeling approach, single maximum value (0.07 mol CO_2 mol^{-1} PPFD) of ε_0 was used to model GPP across all site–years instead of using site- and year-specific maximum ε_0 values.

The T_{scalar} for each time step was estimated as in Terrestrial Ecosystem Model (Raich et al., 1991):

$$T_{scalar} = \frac{(T - T_{\min})(T - T_{\max})}{(T - T_{\min})(T - T_{\max}) - (T - T_{opt})^2} \quad (8)$$

where $T_{\min}$, $T_{\max}$, and T_{opt} represent minimum, maximum and optimal temperature for photosynthesis, respectively. Values of $T_{\min}$, $T_{\max}$, and T_{opt} vary depending on crop type. In this study, $T_{\min}$, T_{opt}, and $T_{\max}$ values were set to −1 °C, 28 °C, and 50 °C, respectively. Study of the relationship between plant development and temperature for soybeans showed the optimum temperature range of about 28–30 °C (Brown, 1960). From the examination of GPP_{EC}–temperature relationship in these flux tower sites, maximum GPP_{EC} was observed at approximately 28 °C (data not shown).

In the situation with LSWI $\geqslant 0$ during the growing season, W_{scalar} was estimated as follows:

$$W_{scalar} = \frac{1 + \mathrm{LSWI}}{1 + \mathrm{LSWI_{max}}} \quad (9)$$

where $LSWI_{max}$ represents the maximum LSWI during the growing season. Mean seasonal cycle of LSWI over the study period was calculated and then the maximum LSWI during the growing season was selected as an estimate of $LSWI_{max}$.

The rain-fed Bondville site experienced severe drought during an early part of the 2002 soybean growing season (mid-June to mid-July), while other study sites did not experience severe drought. To examine the ability of LSWI to track this drought, the seasonal evolution of LSWI for individual years of the study period and also the mean seasonal cycle of LSWI for the soybean growing seasons, even years from 2000 to 2012, were plotted (Fig. 1). Fig. 1 shows that long-term mean LSWI values during 2000–2012 (even years) and LSWI values in 2004 and 2006 were positive during the active growing season, from mid-June to mid-September, but LSWI values in dry periods of 2002 were negative at the Bondville site. To account for the effect of water stress on photosynthesis, a modified approach of W_{scalar} calculation (Eq. (10)) for the drought period (reflected by LSWI < 0 within the plant growing season) has recently been incorporated in VPM (Wagle et al., 2014). As no

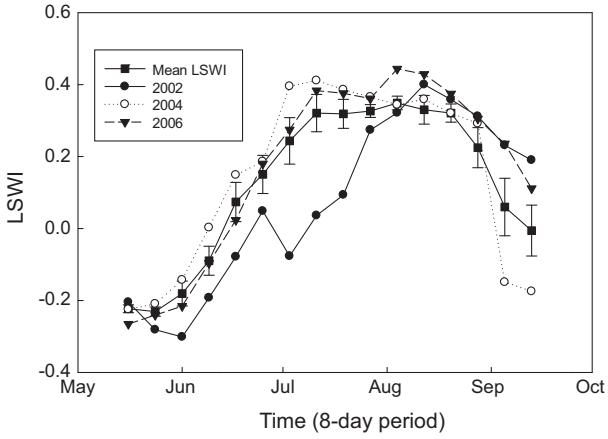

Fig. 1. Seasonal dynamics of MODIS-derived land surface water index (LSWI) at the Bondville site. Mean LSWI represents average LSWI for the soybean growing seasons from 2000 to 2012 (even years).

negative LSWI values within the soybean growing season were observed at the Rosemount and Mead sites, the Eq. (10) was used only at the Bondville site for the period of severe drought (mid-June to mid-July 2002 when LSWI < 0).

$$W_{scalar} = \textit{long-term mean}\ \mathrm{LSWI}_{max} + \mathrm{LSWI} \quad (10)$$

A maximum value of LSWI (0.35) from the mean seasonal cycle of LSWI during the 2000–2012 soybean growing seasons (even years) was used as a long-term mean $LSWI_{max}$. This long-term mean $LSWI_{max}$ helps measure a deviation during drought compared to the normal condition.

2.6. A comparison of GPP_{EC} with the standard MODIS-GPP product (MOD17A2)

The MODIS Land Science Team makes the standard MODIS-GPP/NPP product (MOD17A2) available to the public (Running et al., 1999b), which is computed as follows:

$$\mathrm{GPP}_{\mathrm{MOD17A2}} = \varepsilon \times \mathrm{FPAR} \times \mathrm{PAR} \quad (11)$$

where ε is light use efficiency, FPAR is the fraction of PAR absorbed by the canopy, and PAR is photosynthetically active radiation. In the MODIS-GPP algorithm, two scalars (T_{min}_scalar and VPD_scalar) attenuate ε_{max} (maximum theoretical LUE for each vegetation type) to produce the final ε as follows:

$$\varepsilon = \varepsilon_{max} \times T_{min}\_scalar \times VPD\_scalar \quad (12)$$

FPAR in the MODIS-GPP algorithm comes from the MODIS Leaf Area Index and FPAR 8-day L4 data product (MOD15A2), which is based on the inversion of radiative transfer models and NDVI data (if the inversion of radiative transfer models fails) (Myneni et al., 2002). The MODIS GPP product ($GPP_{MOD17A2}$) has 8-day temporal resolution and 1 km spatial resolution. The $GPP_{MOD17A2}$ (MOD17A2) and FPAR (MOD15A2) data were downloaded from the Oak Ridge National Laboratory Distributed Active Archive Center (ORNL DAAC) website (http://daac.ornl.gov/MODIS/modis.html).

3. Results and discussion

3.1. Seasonal dynamics, magnitudes, and budgets of soybean GPP and NEE

Different magnitudes of NEE and GPP_{EC} were observed across study sites (Fig. 2, Table 1). The GPP_{EC} started to rise (>1 g C m^{-2} day^{-1}) at the beginning of the crop growing season (mid-May or later) and then fell below 1 g C m^{-2} day^{-1} after crop senescence

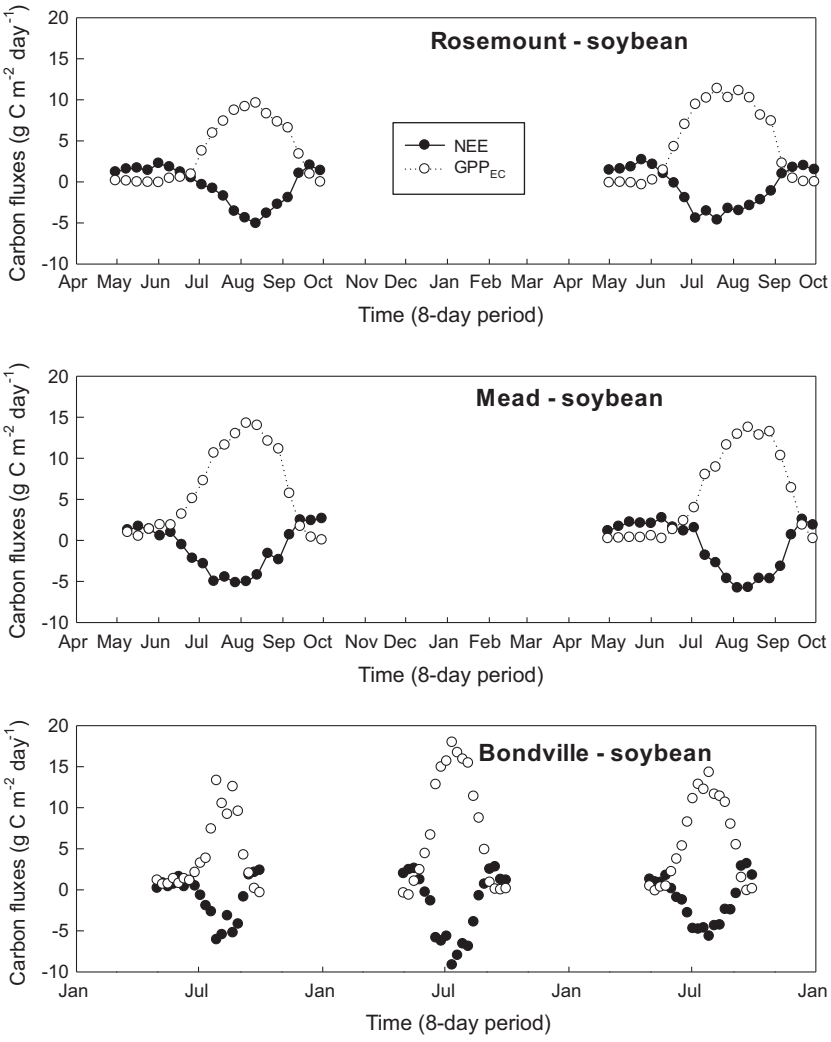

Fig. 2. Seasonal dynamics of net ecosystem CO_2 exchange (NEE) and gross primary production (GPP_{EC}) at three soybean flux sites. Each data point represents an average value of 8-day composites.

Table 1
Seasonal dynamics, magnitudes, and budgets of net ecosystem CO_2 exchange (NEE) and gross primary production (GPP_{EC}), and seasonal (May–October) cumulative rainfall (mm) at three soybean flux sites.

Site – crop	Year	GSL_{VI} (DOY)	CUP (DOY)	GPP_{EC} > 1 g C m^{-2} day^{-1} (DOY)	Max. GPP_{EC} (g C m^{-2} day^{-1})	Max. NEE (g C m^{-2} day^{-1})	May–October sum NEE (GPP)	May–October rainfall
Rosemount – soybean	2004	152–280	184–248	184–264	9.6	−5.06	−37 (586)	571
	2006	144–280	169–241	161–241	11.35	−4.65	−59 (742)	392
Mead – soybean	2002[a]	144–280	169–241	145–257	14.26	−5.16	−141 (936)	637
	2004	152–288	192–248	168–264	13.76	−5.79	−48 (877)	592
Bondville – soybean	2002	144–280	185–249	145–257	13.31	−6.07	−127 (684)	347
	2004	128–280	152–232	136–248	17.96	−9.16	−264 (1194)	481
	2006	128–280	161–249	153–257	14.29	−5.65	−167 (950)	477

DOY represents Day of the Year. Daily NEE and GPP_{EC} values for the period of May to October (soybean growing season) were summed to get seasonal NEE and GPP_{EC} sums (g C m^{-2}).
[a] As NEE and GPP_{EC} data were only available from May 15, 2002 at the Mead site, seasonal sums of NEE and GPP_{EC} were derived from May 15 to the end of October.

(mid-September). The GPP_{EC} was >1 g C m^{-2} day^{-1} for about 81–113 days across the study sites. Generally, the CUP of the ecosystems ranged from 65 to 89 days (2–3 months). July and August were periods of carbon uptake for soybean across all sites. Both GPP_{EC} and NEE reached peak values during mid-July to mid-August.

Slightly smaller magnitudes of GPP_{EC} (9.6–11.35 g C m^{-2} day^{-1}) and NEE (−4.65 to −5.06 g C m^{-2} day^{-1}) were observed at the conventional-till (Rosemount) site compared to no-till Mead and Bondville sites (Fig. 2, Table 1). At the Mead site, GPP_{EC} magnitude ranged from 13.76 to 14.26 g C m^{-2} day^{-1} and NEE magnitude ranged from −5.16 to −5.79 g C m^{-2} day^{-1}. The magnitudes of GPP_{EC} and NEE in 2002 and 2006 at the rainfed Bondville site were similar to those of the irrigated Mead site, except slightly larger GPP_{EC} (17.96 g C m^{-2} day^{-1}) and NEE (−9.16 g C m^{-2} day^{-1}) magnitudes in 2004, a year with well-distributed seasonal rainfall of 481 mm.

The value of integrated NEE and GPP_{EC} at the end of the growing season provides a summary of seasonal carbon budgets of ecosystems. Soybean sites were net sinks of carbon for all site–years (Table 1). However, seasonal carbon budgets exhibited spatial and temporal variability. The rainfed Rosemount site was a small sink of carbon in both years of the study period. The site gained −59 g C m^{-2} during the 2006 growing season when seasonal rainfall was 392 mm, but it gained only −37 g C m^{-2} during the 2004 growing season even though seasonal rainfall was 571 mm. This was because of lack of well-distributed rainfall: 60% of the seasonal rainfall occurred in May and September 2004 while the most active growing period (June–August) was relatively dry (data not shown). Similarly, seasonal sums of NEE and GPP_{EC} were less in the rainfed Bondville site when the site received only 347 mm of seasonal rainfall. However, the Bondville site was a larger sink of carbon even than the irrigated Mead site when it received over 450 mm of well-distributed seasonal (May–October) rainfall. This result is well supported by Fig. 3. Seasonal sums of net ecosystem productivity (NEP = −NEE), GPP_{EC}, and EVI were higher when rainfall was 450–500 mm (Fig. 3), suggesting that rainfed soybean fields needed about 450–500 mm of well-distributed seasonal rainfall to maximize net carbon uptake and to maintain high productivity.

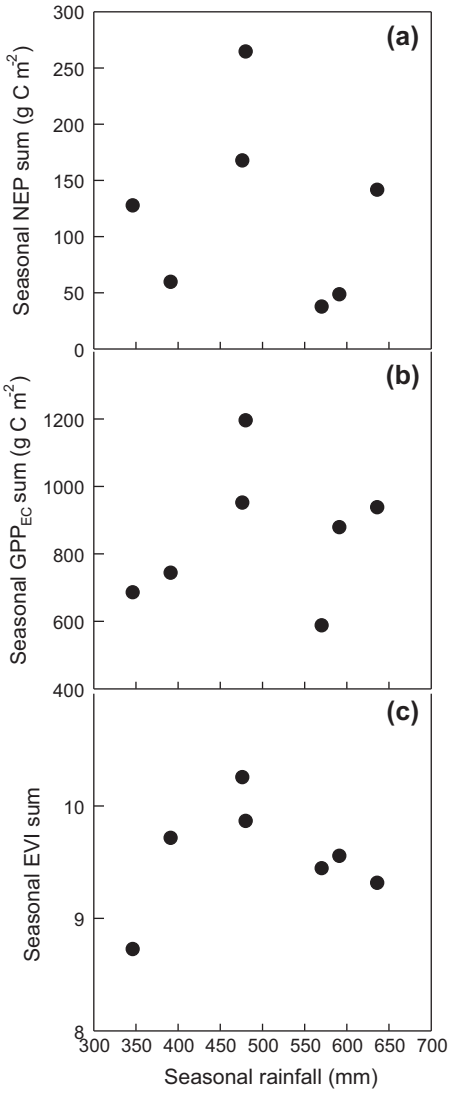

Fig. 3. Relationships between seasonal (May–October) rainfall on seasonal sums of net ecosystem productivity (NEP = −NEE, net ecosystem CO_2 exchange), gross primary production (GPP_{EC}), and enhanced vegetation index (EVI) across three soybean flux sites.

3.2. Seasonal dynamics of VIs

Fig. 4 shows seasonal dynamics of NDVI, EVI, and LSWI for the study sites during the study period. The LSWI values were larger in winter due to snow cover. Values dropped below zero in late spring before soybean planting, started to increase at the beginning of the growing season, and became positive through harvest. Similarly, NDVI and EVI started to increase at the beginning of the growing season (May), reached peak values during peak growth (July–August), and declined after crop senescence or harvest (October). The seasonal distribution of VIs followed that of the carbon fluxes.

For a better characterization of the seasonal dynamics of soybean NDVI, EVI, and LSWI, mean seasonal cycles of NDVI, EVI,

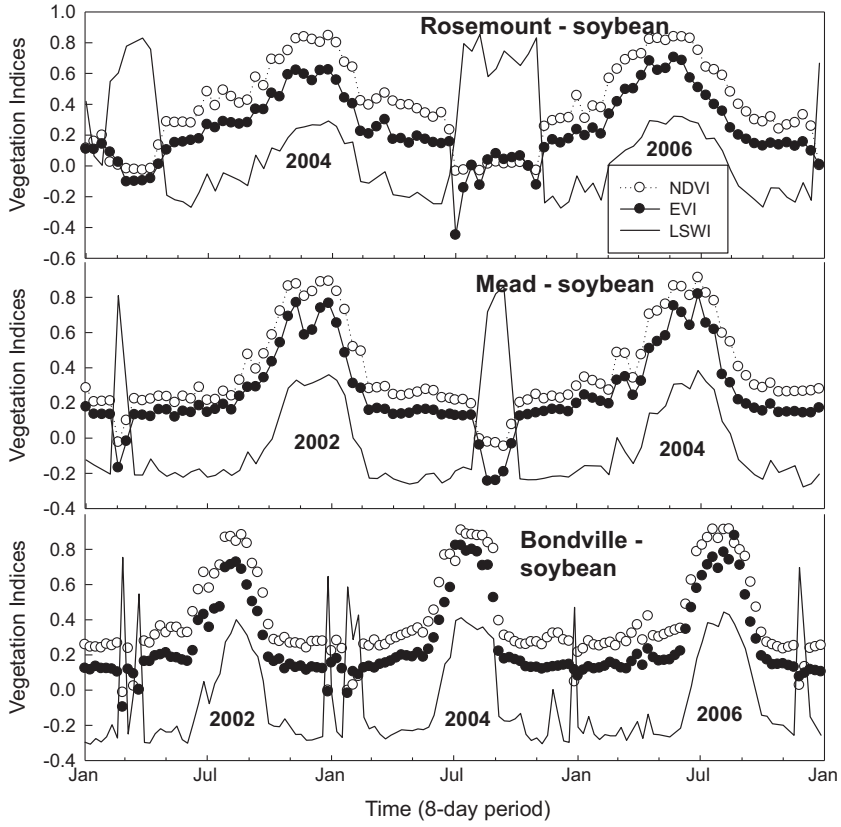

Fig. 4. Seasonal dynamics of MODIS-derived vegetation indices (NDVI, EVI, and LSWI) for the study period at three soybean flux sites.

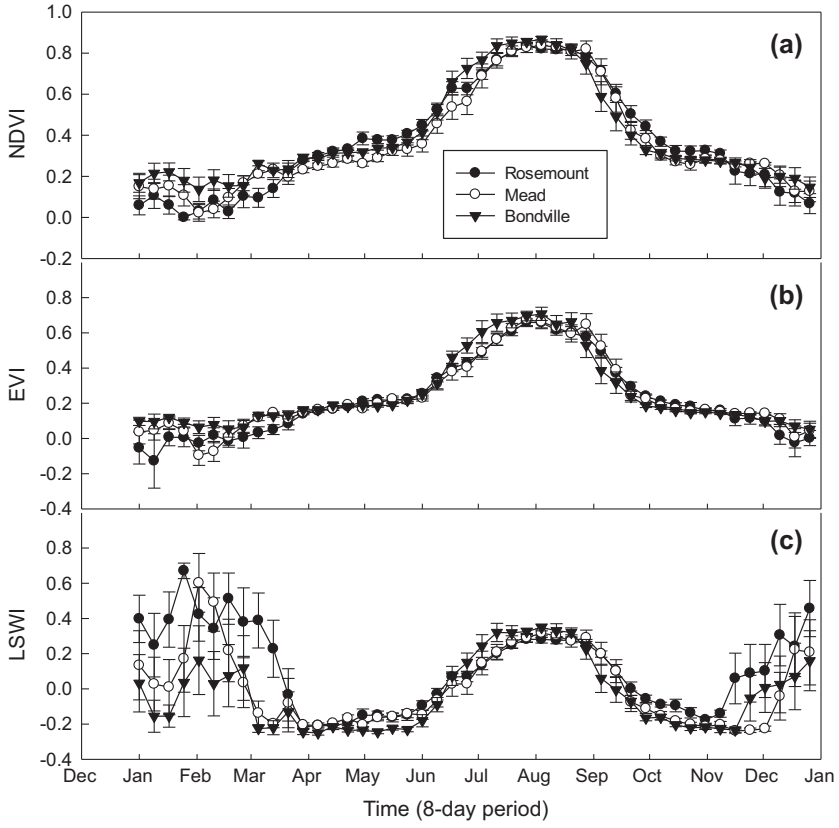

Fig. 5. A comparison of seasonal mean cycles of MODIS-derived vegetation indices (NDVI, EVI, and LSWI) based on soybean growing years (even years from 2000 to 2012) for three soybean flux sites.

and LSWI were determined based on seven years of available data for the soybean growing seasons (even years from 2000 to 2012) and compared across three locations (Fig. 5). All three VIs followed similar temporal patterns and magnitudes during the soybean growing season across all soybean sites. The maximum NDVI, EVI, and LSWI values across three sites ranged between 0.83 and 0.87, 0.66 and 0.70, and 0.28 and 0.35, respectively.

3.3. Correlation of GSL from remote sensing with the CUP and seasonal sums of NEE and GPP_{EC}

It is well known that the CUP starts after a certain period of vegetation growth once the vegetation is large enough to photosynthesize at a higher rate than the rate of ER, and the CUP terminates when ER is higher than GPP even though vegetation growth continues (Churkina et al., 2005). As a result, GSL_{VI} was longer than the CUP for each site–year (Table 1). However, as the seasonal dynamics of carbon fluxes corresponded well with the vegetation dynamics, regression analysis showed a strong linear relationship ($R^2 = 0.84$) between the CUP and GSL_{VI} (Fig. 6). Similarly, GSL_{VI} was strongly correlated with the seasonal sums of NEP (net ecosystem production = −NEE, $R^2 = 0.78$) and GPP ($R^2 = 0.54$). The results suggest that the length of the vegetation activity period derived from satellite-derived NDVI and EVI can be inferred to determine the CUP and seasonal sums of NEE and GPP, consistent with a previous study (Churkina et al., 2005).

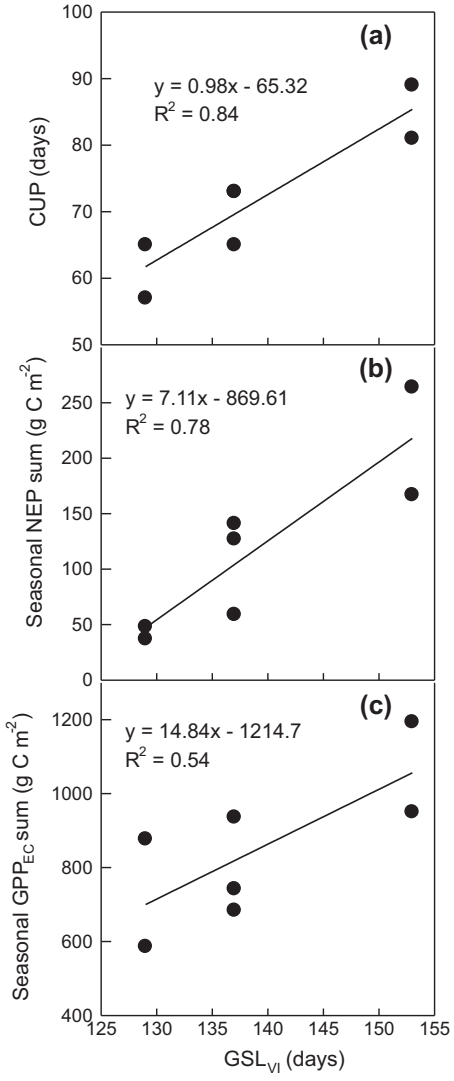

Fig. 6. Relationships between growing season length based on vegetation indices (GSL_{VI}), carbon uptake period (CUP), and seasonal sums of net ecosystem productivity (NEP = −NEE, net ecosystem CO_2 exchange) and gross primary production (GPP_{EC}) across three soybean flux sites.

3.4. Relationships between VIs and GPP_{EC}

Strong relationships between VIs (NDVI and EVI) and GPP_{EC} were observed at all sites (Fig. 7). The results indicate that EVI had a slightly stronger linear relationship with GPP_{EC} than did NDVI, consistent with previous studies in forests (Xiao et al., 2004a,b), upland crops (winter wheat and maize) (Kalfas et al., 2011; Yan et al., 2009), and grasslands (Li et al., 2007; Wagle et al., 2014). Since NDVI has been widely used for remote sensing based applications, these findings indicate that the use of EVI instead of NDVI could provide better results for remote sensing based applications.

3.5. Seasonal dynamics of GPP as predicted by VPM

The seasonal dynamics of GPP_{VPM} were compared with the GPP_{EC} over the soybean growing seasons (Fig. 8). Seasonal dynamics of GPP_{VPM} agreed reasonably well with those of GPP_{EC}. However, there still exist large differences between GPP_{VPM} and GPP_{EC} for a few 8-day periods. These discrepancies might be attributed to three error sources. The first error source is the sensitivity of the GPP_{VPM} to weather data (temperature, PAR or PPFD). For example, VPM predicts higher GPP_{VPM} at higher PPFD. But that might not always be true as the response of CO_2 flux to PPFD varies under different climatic conditions. It was well supported by the observed different responses of NEE to PPFD at the Bondville site during mid-June to mid-July for 2002 and 2004 (Fig. 9). It is important to note that the Bondville site is a rainfed agriculture system. In 2004 when there was no drought, NEE increased with increasing PPFD and no indication of NEE saturation was observed up to 2000 μmol m^{-2} s^{-1} PPFD. But during drought in 2002, the maximum NEE was observed at PPFD levels of 1000–1500 μmol m^{-2} s^{-1} and NEE decreased considerably when PPFD increased further. The second error source is uncertainty in estimation of GPP_{EC} as GPP_{EC} is calculated as the residual between measured NEE and modeled daytime ER. Daytime ER modeling and NEE measurements by eddy covariance systems introduce some error and uncertainty. Thus, it is difficult to assess all error and uncertainty introduced. The third error source is time-series data of satellite-derived VIs. The 8-day MODIS composite image has no bidirectional reflectance distribution function (BRDF) correction or normalization to account for the effect of angular geometry on surface reflectance and VIs. The composite procedure used in the production of MOD09A1 also affects the results. The first and second sources of error are most likely to have the greater influence on the discrepancy between GPP_{VPM} and GPP_{EC}. However, further investigations are necessary to determine the relative role of individual sources of error.

Overall, there is good agreement between GPP_{VPM} and GPP_{EC} (Table 2). Values of integrated GPP_{VPM} over the growing season were 591 g C m^{-2} in 2004 and 808 g C m^{-2} in 2006 at the Rosemount site, while seasonal totals of GPP_{EC} were 569 and 745 g C m^{-2} in the respective years (Table 3). The results indicate that the model overestimated GPP by 4% and 8% in 2004 and 2006, respectively. At the Mead site, growing season integrated GPP_{VPM} was 1% and 8% lower than GPP_{EC} in 2002 and 2004, respectively. At the Bondville site, the model overestimated GPP by 22% in 2002, and underestimated by 17% and 4% in 2004 and 2006, respectively. Larger discrepancies between GPP_{EC} and GPP_{VPM} in 2002 and 2004 as compared to 2006 can be explained by the drastically different patterns of NEE and GPP for those years (Fig. 10).

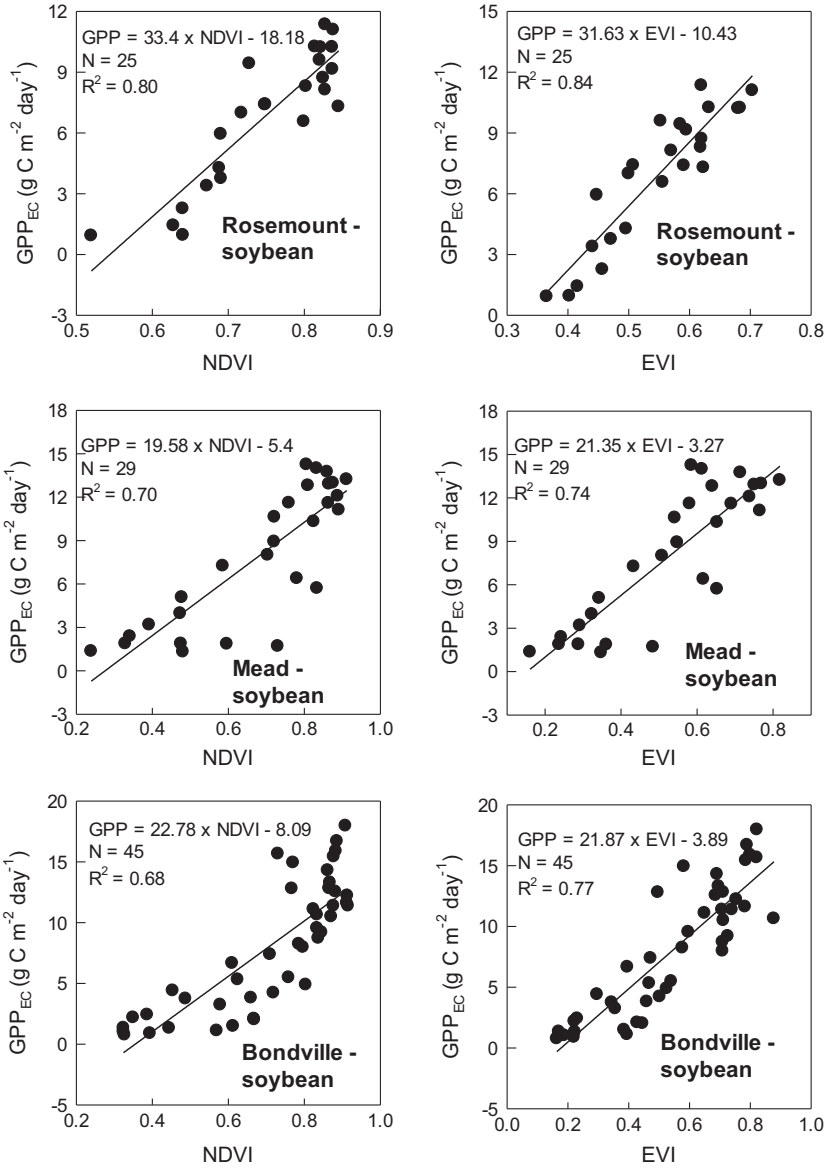

Fig. 7. Relationships between vegetation indices (normalized difference vegetation index, NDVI, and enhanced vegetation index, EVI) and gross primary production (GPP_{EC}) during the active growing season (GPP > 1 g C m^{-2} day^{-1}) at three soybean flux sites. Simple linear regression models were highly significant ($P < 0.0001$).

The ecosystem did not start to gain carbon (negative NEE) until the first week of July in 2002 because the crop was not planted till 2nd June while normally it is planted in early to mid-May. Also the site experienced a severe drought from mid-June through mid-July 2002. In contrast, the site started gaining carbon a month earlier (1st week of June) in 2004 and three weeks earlier (2nd week of July) in 2006. The GPP_{EC} started to rise earlier and attained larger magnitude in 2004 while it was heavily suppressed until mid-July in 2002. This over- or under-estimation of GPP_{EC} in 2002 and 2004 was partly explained by a smaller difference in EVI, but a larger difference in GPP_{EC} over the years (Fig. 10). For example, GPP_{EC} in mid-July was 12.82 g C m^{-2} day^{-1} in 2006 while it was 3.82 g C m^{-2} day^{-1} (70% lower) in 2002 and 17.96 g C m^{-2} day^{-1} (40% higher) in 2004. In contrast, EVI in mid-July was 0.71 in 2006 while it was 0.46 (35% lower) in 2002 and 0.82 (16% higher) in 2004. This result showed that change in EVI was about two folds smaller than that of GPP_{EC}, suggesting that GPP is more sensitive to weather conditions (extremely favorable or unfavorable) than EVI.

To further examine the sensitivity of GPP to drought, diurnal patterns of GPP_{EC} and major environmental drivers [PPFD, air temperature, and vapor pressure deficit (VPD)] were compared for drought and non-drought periods at the Bondville site (Fig. 11). During drought with high VPD, GPP_{EC} increased rapidly after sunrise following the trend of PPFD and then decreased suddenly at around 8:00 AM when VPD reached ~1.2 kPa. The GPP_{EC} again started to increase in the afternoon and reached the second peak at 4:00 PM after VPD started to decline. The VPD reached a peak (2.5 kPa) at 3:00 PM. As a result, GPP_{EC} showed a bimodal distribution (Fig. 11a). A symmetrical diurnal GPP_{EC} cycle with a unimodal distribution following the same pattern of PPFD was observed when the maximum VPD was smaller than 1.2 kPa during a non-drought period (Fig. 11b). These results illustrated that VPD > 1.2 kPa started to limit photosynthesis in soybean via stomatal regulation. Bunce (1984) showed decreased stomatal conductance in soybean at VPD of 3 kPa compared with 1 kPa. The results indicate that overestimation of GPP by the model during the period of higher VPD (drought) can be attributed to the inability of the model to account for the pronounced midday depression of GPP_{EC} as shown in Fig. 11a. Gilmanov et al. (2014) also reported strong limitation of plant productivity of legumes

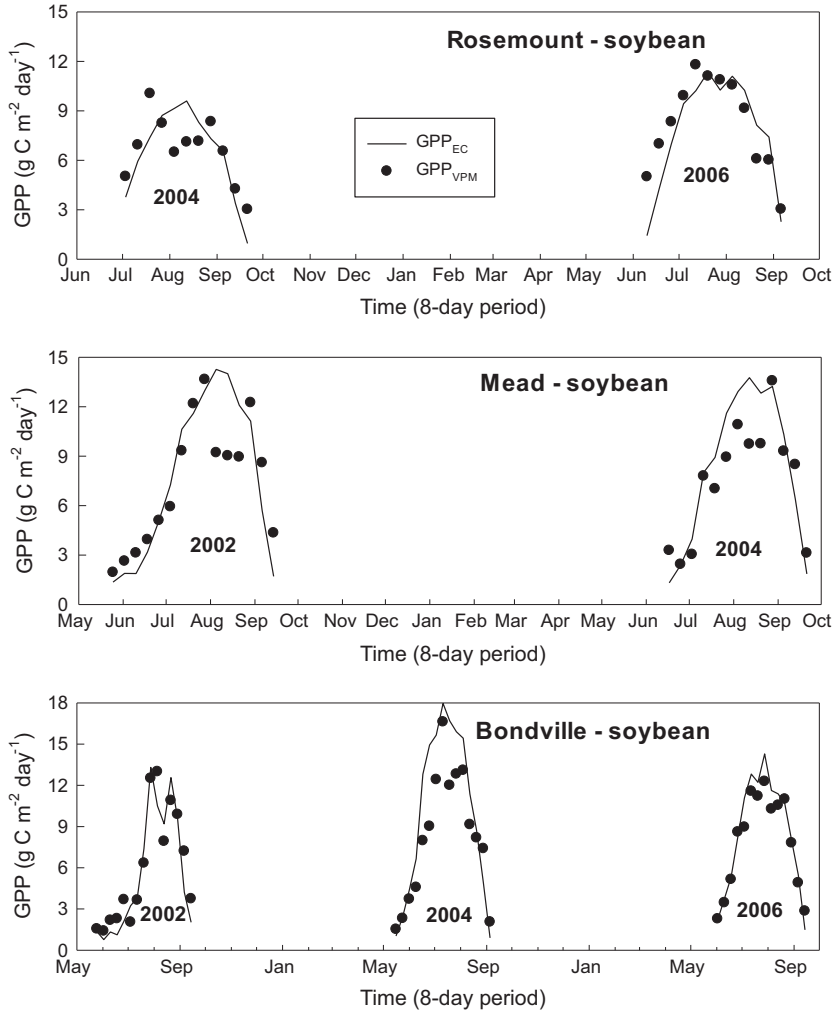

Fig. 8. A comparison of seasonal dynamics and interannual variations of gross primary production from flux tower (GPP_{EC}) and vegetation photosynthesis model (GPP_{VPM}) at three soybean flux sites.

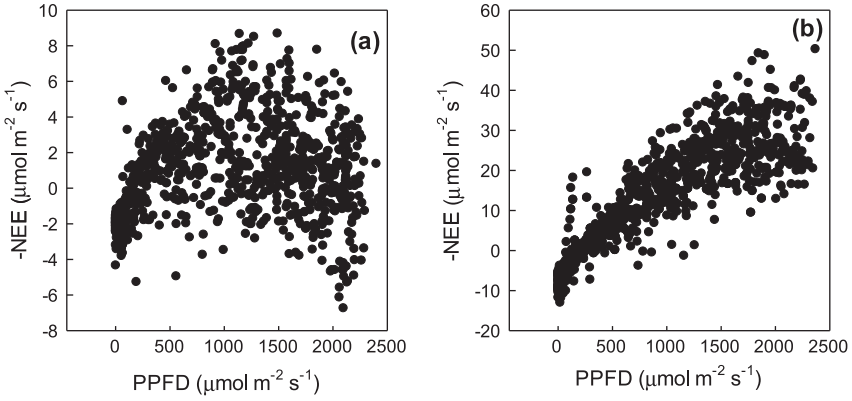

Fig. 9. Relationship between soybean net ecosystem CO_2 exchange (NEE) to photosynthetic photon flux density (PPFD) during mid-June to mid-July 2002 (a) and 2004 (b) at the Bondville site.

including soybean in periods of water deficit and higher VPD. The limitation of canopy CO_2 exchange necessitated the modification of the classical rectangular or nonrectangular hyperbolic light-PPFD equation by introducing the VPD-dependent control of photosynthetic uptake (Gilmanov et al., 2014; Lasslop et al., 2010; Wagle and Kakani, 2014b).

During drought, several environmental factors (high PPFD, VPD, and temperature, and low soil water content) are tightly linked to each other and can exert confounding effects on the sensitivity of CO_2 fluxes to these controlling factors (Wagle and Kakani, 2014a). Interestingly, LSWI tracked drought well (Fig. 1). With the modified approach of W_{scalar} calculation in VPM, the model

performance improved substantially in 2002 at the Bondville site: R^2 value for the simple linear regression between GPP_{EC} and GPP_{VPM} increased from 0.76 to 0.89 (Table 2) and overestimation of GPP dropped down to 7% from 22% (Table 3). Similarly, RMSE and MAE dropped from 2.3 to 1.43 g C m^{-2} and from 1.85 to 1.21 g C m^{-2}, respectively (Table 3).

A number of investigators have explored and coined different names for remote sensing products related to canopy water content or water stress. For example, normalized difference infrared index (NDII) (Yilmaz et al., 2008), normalized difference of Landsat TM bands 4 and 5 (ND45) (Kimes et al., 1981), shortwave infrared water stress index [SIWSI(6,2)] (Fensholt and Sandholt, 2003), and normalized difference water index (NDWI) (Jackson et al., 2004; Maki et al., 2004). The LSWI used in this study employs the normalized difference between the NIR (0.78–0.89 μm) and SWIR (1.58–1.75 μm) spectral bands (Xiao et al., 2004a). There is a need to use a single term in the community, which could reduce confusion among the users. It is also necessary to further evaluate and compare those indices that use different spectral near infrared and shortwave infrared bands.

3.6. Seasonal dynamics of MODIS-GPP ($GPP_{MOD17A2}$) product

A comparison of $GPP_{MOD17A2}$ and GPP_{EC} shows that $GPP_{MOD17A2}$ was substantially lower than GPP_{EC} (Fig. 12). $GPP_{MOD17A2}$ also did not follow the clear seasonal trend observed in GPP_{EC} for the Rosemount and Mead sites. As a result, $GPP_{MOD17A2}$ showed poor relationships with EVI ($R^2 = 0.14$ at the Rosemount site and

Table 2
Linear regression coefficients and coefficient of determination (R^2) of gross primary production from flux tower (GPP_{EC}), vegetation photosynthesis model (GPP_{VPM}), and MODIS GPP ($GPP_{MOD17A2}$) for three soybean flux sites.

Site – crop	Year	$GPP_{EC} = a \times GPP_{VPM}$		$GPP_{EC} = a \times GPP_{MOD17A2}$	
		Slope	R^2	Slope	R^2
Rosemount – soybean	2004	0.97	0.58	1.16	0.55
	2006	0.93	0.75	1.49	0.16
	Two years	0.94	0.70	1.32	0.25
Mead – soybean	2002	1.03	0.76	2.51	0.09
	2004	1.10	0.85	2.1	0.49
	Two years	1.06	0.80	2.25	0.24
Bondville – soybean	2002	0.96 (0.88)	0.89 (0.76)	1.09	0.62
	2004	1.20	0.89	1.68	0.73
	2006	1.06	0.96	1.46	0.78
	Three years	1.1	0.89	1.42	0.66

Two different approaches (Eqs. (9) and (10)) of W_{scalar} (a down-regulation scalar to account for the effect of water stress on GPP) calculation was used for normal and drought periods, respectively. Slope and R^2 value in brackets () represent the results when W_{scalar} was determined based on Eq. (9) during drought.

Table 3
Seasonally integrated sums of tower based (GPP_{EC}), modeled (GPP_{VPM}), and MODIS ($GPP_{MOD17A2}$) gross primary production (g C m^{-2}), root mean square error (RMSE, g C m^{-2}), and mean absolute error (MAE, g C m^{-2}) for three soybean flux sites.

Site – crop	Year	GPP_{EC}	GPP_{VPM}	MAE	RMSE	$GPP_{MOD17A2}$	MAE	RMSE
Rosemount – soybean	2004	569	591	1.45	1.70	495	1.78	1.98
	2006	745	808	1.43	1.74	499	3.47	3.96
Mead – soybean	2002	918	906	1.86	2.33	364	5.28	6.53
	2004	860	791	1.61	1.95	423	4.7	5.61
Bondville – soybean	2002	660	706 (806)	1.21 (1.85)	1.43 (2.30)	672	2.28	2.7
	2004	1198	996	2.26	2.80	760	4.41	5.47
	2006	948	906	0.74	0.93	676	2.96	3.45

Two different approaches (Eqs. (9) and (10)) of W_{scalar} (a down-regulation scalar to account for the effect of water stress on GPP) calculation was used for normal and drought periods, respectively. GPP_{VPM}, MAE, and RMSE values in brackets () represent results when W_{scalar} was determined based on Eq. (9) during drought. Each value of GPP_{VPM} and $GPP_{MOD17A2}$ were multiplied by eight (days) and summed to obtain seasonal values for the period of $GPP_{EC} > 1$ g C m^{-2} day^{-1}.

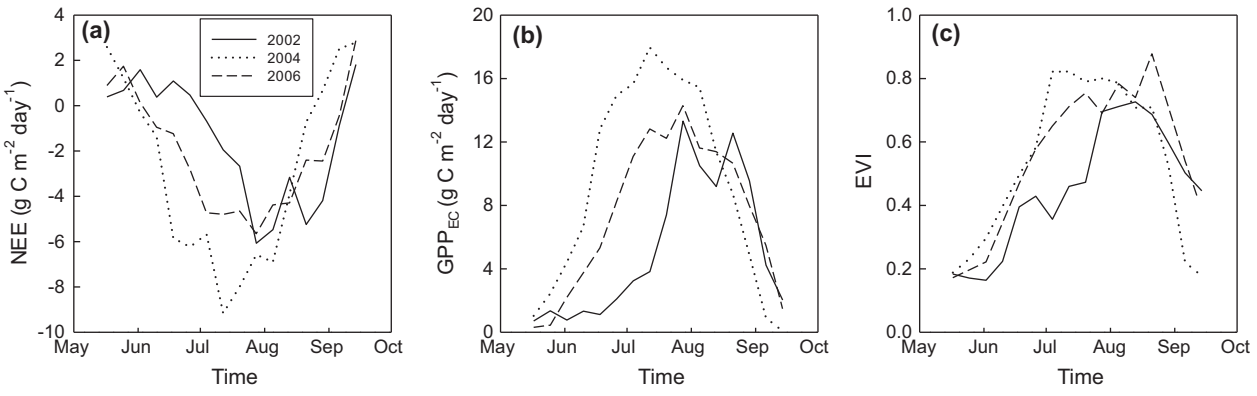

Fig. 10. Seasonal dynamics of soybean net ecosystem CO_2 exchange (NEE), gross primary production (GPP_{EC}), and enhanced vegetation index (EVI) at the Bondville site.

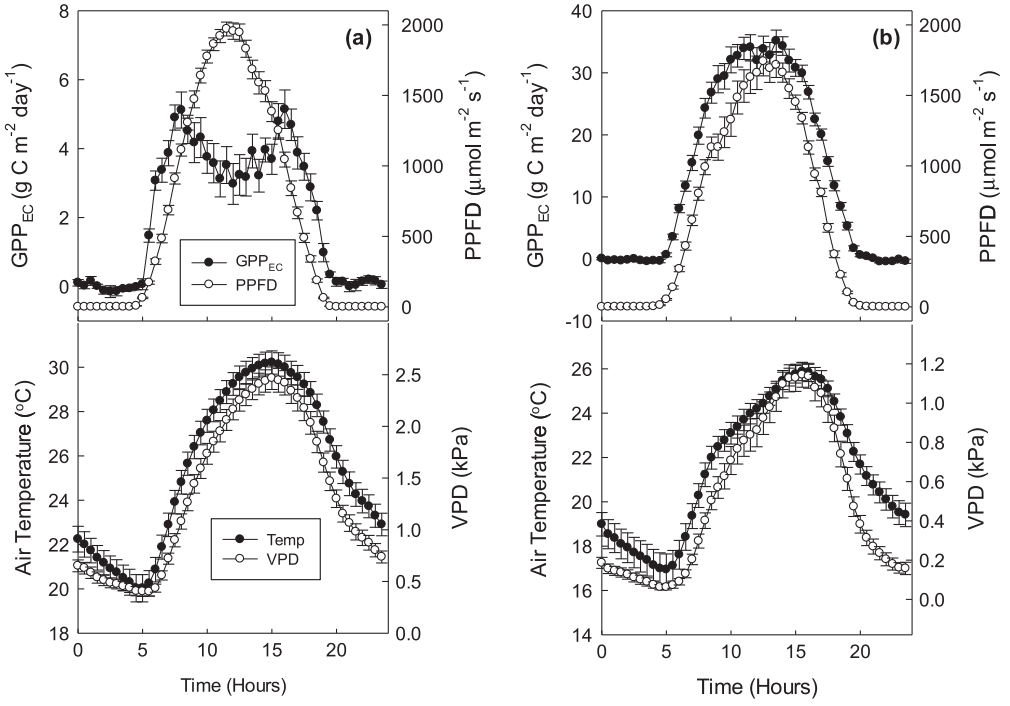

Fig. 11. Relationship between soybean gross primary production (GPP_{EC}) and photosynthetic photon flux density (PPFD), air temperature (Temp), and vapor pressure deficit (VPD) during mid-June to mid-July 2002 (a) and 2004 (b) at the Bondville site. Bars represent standard errors of the means.

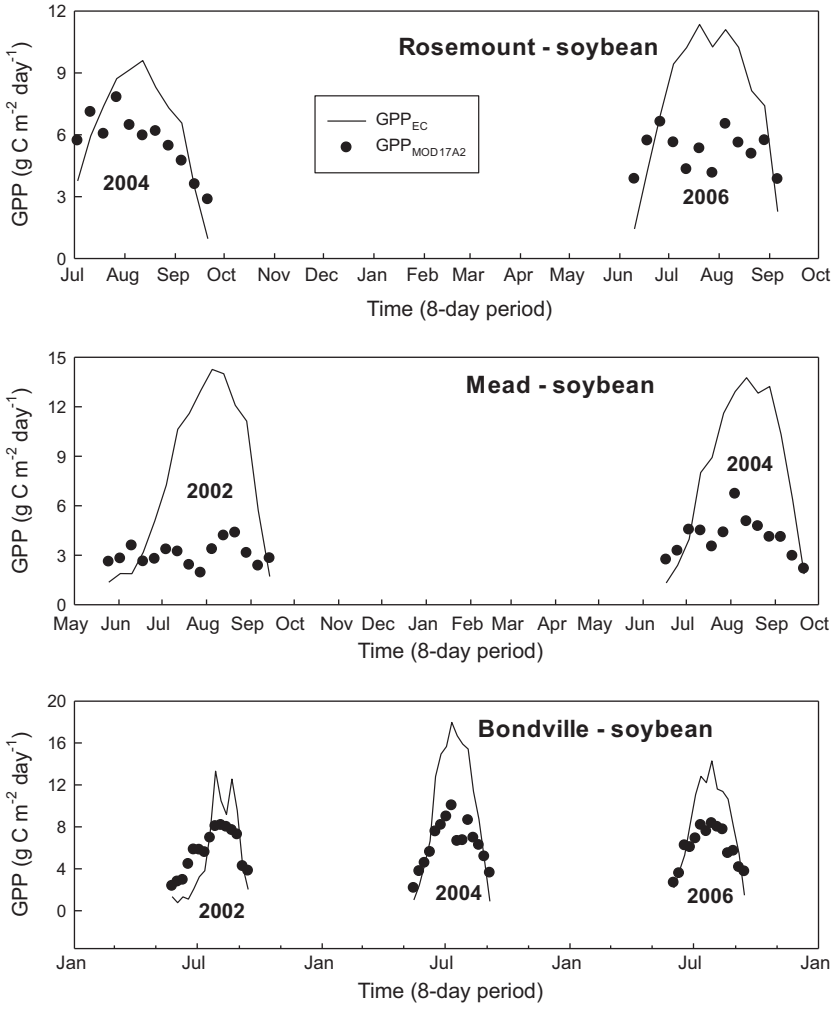

Fig. 12. A comparison of the seasonal dynamics and interannual variations of flux tower gross primary production (GPP_{EC}) and MODIS GPP ($GPP_{MOD17A2}$) at three soybean flux sites.

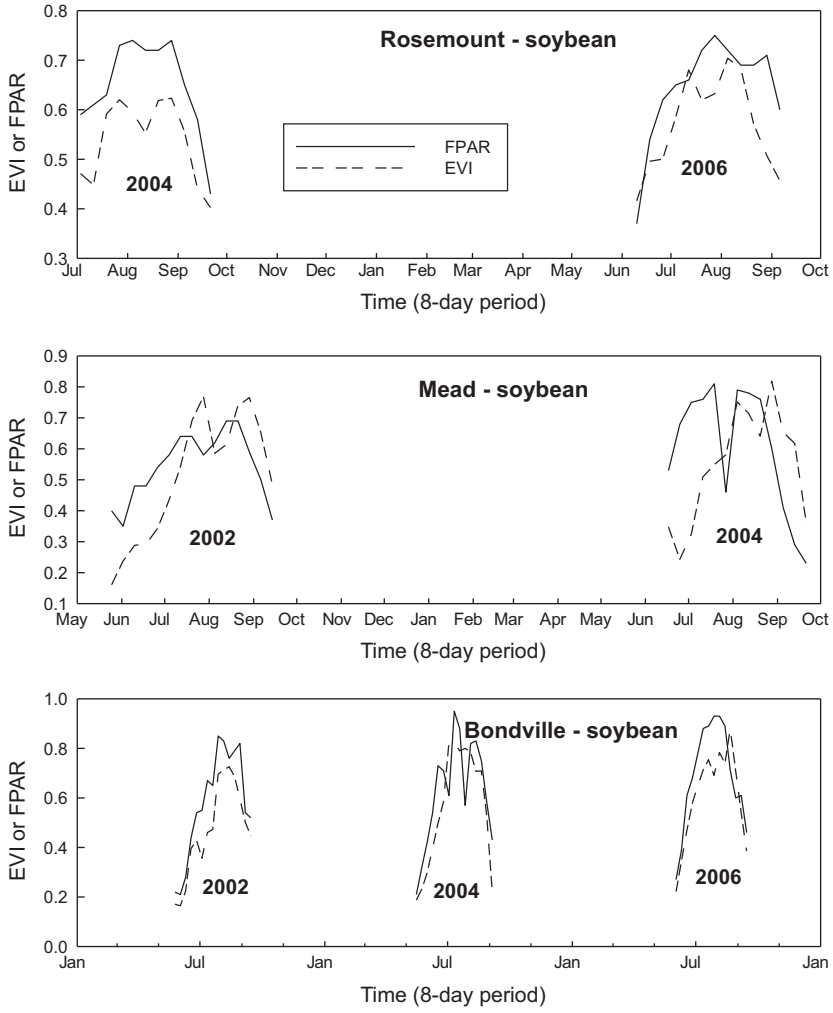

Fig. 13. A comparison of MODIS-derived fraction of absorbed radiation by canopy (FPAR) and enhanced vegetation index (EVI) at three soybean flux sites.

$R^2 = 0.13$ at the Mead site) while GPP_{EC} and GPP_{VPM} had strong linear relationships with EVI (GPP_{EC} vs. EVI: $R^2 = 0.84$ at the Rosemount site and $R^2 = 0.74$ at the Mead site, Fig. 7; GPP_{VPM} vs. EVI: $R^2 = 0.66$ at the Rosemount site and $R^2 = 0.90$ at the Mead site). $GPP_{MOD17A2}$ also showed poor relationships with FPAR ($R^2 = 0.27$ at the Rosemount site and $R^2 = 0.37$ at the Mead site) at these sites. There were also clear differences in the seasonal evolution of FPAR and EVI at the Rosemount and Mead sites, especially an early rise of FPAR in the spring (Fig. 13). Because of this FPAR effect, $GPP_{MOD17A2}$ started its spring rise early across all site–years, consistent with previous studies (Turner et al., 2005, 2006). Relatively similar patterns of FPAR and EVI at the Bondville site resulted in strong relationships of $GPP_{MOD17A2}$ with FPAR ($R^2 = 0.81$) and EVI ($R^2 = 0.71$). However, the magnitude of $GPP_{MOD17A2}$ was still substantially lower than that of GPP_{EC}. Note that GPP_{VPM} followed similar seasonal trends and magnitude of GPP_{EC} across the sites (Fig. 8). Large discrepancies of $GPP_{MOD17A2}$ with GPP_{VPM} can be traced to differences in input parameters of VPM and MODIS GPP algorithm (Eqs. (4) and (11), respectively). Consistently larger FPAR than EVI across all site–years (Fig. 13), but substantially smaller $GPP_{MOD17A2}$ as compared to GPP_{VPM} indicates that such underestimation of $GPP_{MOD17A2}$ is associated with low value for vegetation LUE (ε) in the MODIS GPP algorithm. The MODIS GPP algorithm uses ε value of 0.15 g C mol^{-1} PPFD for all grasslands and croplands on the assumption that biome-specific maximum theoretical maximum LUE (ε_{max}) do not vary with space or time. However, it has been shown that LUE in fact varies widely among biome types and in response to environmental conditions (Gower et al., 1999; Scott Green et al., 2003). The tower-based ε_0 value, derived from the NEE-PPFD relationship (one week data) at the peak growth, used for the GPP_{VPM} estimations in this study was 0.84 g C mol^{-1} PPFD. Since eddy flux tower sites provide a strong rationale for validation and parameterization of the MODIS GPP product (Turner et al., 2006), this study suggests that more comprehensive validation of the MODIS products and MODIS algorithm parameters is needed at an increasing number of flux tower sites, particularly cropland and grassland sites.

4. Conclusions

Carbon dioxide flux data from three soybean fields under different management practices (no-till vs. till; irrigated vs. rainfed) were analyzed, and the GPP derived from eddy covariance measurements (GPP_{EC}) was compared against the modeled GPP (GPP_{VPM}) using a satellite-based VPM. The eddy flux measurements showed that the soybean fields have distinct spatial and temporal dynamics of carbon fluxes. Seasonally integrated NEE ranged widely from −37 to −264 g C m^{-2} across soybean sites. Well-distributed seasonal (May–October) rainfall of about 450–500 mm was needed for the rainfed soybean sites to maximize the net carbon sink. The results show that the CUP and seasonal sums of

NEE and GPP can be inferred from the length of the vegetation activity period from satellite remote sensing data. Similarly, strong correlations between GPP_{EC} and VIs indicated the potential use of remote sensing VIs to upscale site-specific GPP measurements over the large soybean areas. On a growing season scale, integrated sums of GPP_{VPM} were generally within ±10% of the integrated sums of GPP_{EC} of soybean fields under different management practices. However, some large discrepancies between GPP_{VPM} and GPP_{EC} were observed under drought conditions when GPP_{EC} was suppressed more heavily than VI. As LSWI tracked drought-impacted vegetation, a modified W_{scalar} in VPM, for the period of LSWI < 0 within the soybean growing season, helped quantify the reduction in GPP during severe droughts and it in turn improved VPM's performance substantially. The results of this study demonstrate the potential use of remotely sensed VIs for better understanding of carbon dynamics and extrapolation of GPP_{EC} of soybean croplands.

Acknowledgments

This study was supported in part by a research grant (Project No. 2012-02355) through the USDA National Institute for Food and Agriculture (NIFA)'s Agriculture and Food Research Initiative (AFRI), Regional Approaches for Adaptation to and Mitigation of Climate Variability and Change, and a research grant from the National Science Foundation EPSCoR (IIA-1301789). We would like to thank Drs. Timothy J. Griffis (University of Minnesota), John M. Baker (USDA ARS), and Tilden P. Meyers (NOAA/ARL) for providing eddy flux data for the study sites and suggestions on the early draft of the manuscript.

Appendix A. Supplementary material

Supplementary data associated with this article can be found, in the online version, at http://dx.doi.org/10.1016/j.isprsjprs.2014.10.009.

References

Angers, D., Bolinder, M., Carter, M., Gregorich, E., Drury, C., Liang, B., Voroney, R., Simard, R., Donald, R., Beyaert, R., 1997. Impact of tillage practices on organic carbon and nitrogen storage in cool, humid soils of eastern Canada. Soil Till. Res. 41, 191–201.

Baker, J., Griffis, T., 2005. Examining strategies to improve the carbon balance of corn/soybean agriculture using eddy covariance and mass balance techniques. Agric. Forest Meteorol. 128, 163–177.

Baldocchi, D., Falge, E., Gu, L., Olson, R., Hollinger, D., Running, S., Anthoni, P., Bernhofer, C., Davis, K., Evans, R., 2001. FLUXNET: a new tool to study the temporal and spatial variability of ecosystem-scale carbon dioxide, water vapor, and energy flux densities. Bull. Am. Meteorol. Soc. 82, 2415–2434.

Brown, D.M., 1960. Soybean ecology. I. Development–temperature relationships from controlled environment studies. Agron. J. 52, 493–496.

Bunce, J.A., 1984. Identifying soybean lines differing in gas exchange sensitivity to humidity. Ann. Appl. Biol. 105, 313–318.

Churkina, G., Schimel, D., Braswell, B.H., Xiao, X., 2005. Spatial analysis of growing season length control over net ecosystem exchange. Global Change Biol. 11, 1777–1787.

Falge, E., Baldocchi, D., Tenhunen, J., Aubinet, M., Bakwin, P., Berbigier, P., Bernhofer, C., Burba, G., Clement, R., Davis, K.J., 2002. Seasonality of ecosystem respiration and gross primary production as derived from FLUXNET measurements. Agric. Forest Meteorol. 113, 53–74.

Fensholt, R., Sandholt, I., 2003. Derivation of a shortwave infrared water stress index from MODIS near-and shortwave infrared data in a semiarid environment. Remote Sens. Environ. 87, 111–121.

Gilmanov, T.G., Baker, J.M., Bernacchi, C.J., Billesbach, D.P., Burba, G.G., Castro, S., Chen, J., Eugster, W., Fischer, M.L., Gamon, J.A., 2014. Productivity and carbon dioxide exchange of leguminous crops: estimates from flux tower measurements. Agron. J. http://dx.doi.org/10.2134/agronj2013.0270.

Goulden, M.L., Daube, B.C., Fan, S.M., Sutton, D.J., Bazzaz, A., Munger, J.W., Wofsy, S.C., 1997. Physiological responses of a black spruce forest to weather. J. Geophys. Res. D: Atmos. 102, 28987–28996.

Gower, S.T., Kucharik, C.J., Norman, J.M., 1999. Direct and indirect estimation of leaf area index, fAPAR, and net primary production of terrestrial ecosystems. Remote Sens. Environ. 70, 29–51.

Griffis, T., Zhang, J., Baker, J., Kljun, N., Billmark, K., 2007. Determining carbon isotope signatures from micrometeorological measurements: implications for studying biosphere–atmosphere exchange processes. Boundary-Layer Meteorol. 123, 295–316.

Hollinger, S.E., Bernacchi, C.J., Meyers, T.P., 2005. Carbon budget of mature no-till ecosystem in North Central Region of the United States. Agric. Forest Meteorol. 130, 59–69.

Huete, A., Didan, K., Miura, T., Rodriguez, E.P., Gao, X., Ferreira, L.G., 2002. Overview of the radiometric and biophysical performance of the MODIS vegetation indices. Remote Sens. Environ. 83, 195–213.

Jackson, T.J., Chen, D., Cosh, M., Li, F., Anderson, M., Walthall, C., Doriaswamy, P., Hunt, E., 2004. Vegetation water content mapping using Landsat data derived normalized difference water index for corn and soybeans. Rem. Sens. Environ. 92, 475–482.

Kalfas, J.L., Xiao, X., Vanegas, D.X., Verma, S.B., Suyker, A.E., 2011. Modeling gross primary production of irrigated and rain-fed maize using MODIS imagery and CO_2 flux tower data. Agric. Forest Meteorol. 151, 1514–1528.

Kimes, D., Markham, B., Tucker, C., McMurtrey III, J., 1981. Temporal relationships between spectral response and agronomic variables of a corn canopy. Remote Sens. Environ. 11, 401–411.

Lasslop, G., Reichstein, M., Papale, D., Richardson, A.D., Arneth, A., Barr, A., Stoy, P., Wohlfahrt, G., 2010. Separation of net ecosystem exchange into assimilation and respiration using a light response curve approach: critical issues and global evaluation. Global Change Biol. 16, 187–208.

Li, Z.Q., Yu, G.R., Xiao, X.M., Li, Y.N., Zhao, X.Q., Ren, C.Y., Zhang, L.M., Fu, Y.L., 2007. Modeling gross primary production of alpine ecosystems in the Tibetan Plateau using MODIS images and climate data. Remote Sens. Environ. 107, 510–519.

Mahadevan, P., Wofsy, S.C., Matross, D.M., Xiao, X.M., Dunn, A.L., Lin, J.C., Gerbig, C., Munger, J.W., Chow, V.Y., Gottlieb, E.W., 2008. A satellite-based biosphere parameterization for net ecosystem CO_2 exchange: vegetation photosynthesis and respiration model (VPRM). Global Biogeochem. Cycles 22, GB2005.

Maki, M., Ishiahra, M., Tamura, M., 2004. Estimation of leaf water status to monitor the risk of forest fires by using remotely sensed data. Remote Sens. Environ. 90, 441–450.

Meyers, T.P., Hollinger, S.E., 2004. An assessment of storage terms in the surface energy balance of maize and soybean. Agric. Forest Meteorol. 125, 105–115.

Myneni, R., Hoffman, S., Knyazikhin, Y., Privette, J., Glassy, J., Tian, Y., Wang, Y., Song, X., Zhang, Y., Smith, G., 2002. Global products of vegetation leaf area and fraction absorbed PAR from year one of MODIS data. Remote Sens. Environ. 83, 214–231.

Potter, C.S., Randerson, J.T., Field, C.B., Matson, P.A., Vitousek, P.M., Mooney, H.A., Klooster, S.A., 1993. Terrestrial ecosystem production: a process model based on global satellite and surface data. Global Biogeochem. Cycles 7, 811–841.

Raich, J., Rastetter, E., Melillo, J., Kicklighter, D., Steudler, P., Peterson, B., Grace, A., Moore III, B., Vorosmarty, C., 1991. Potential net primary productivity in South America: application of a global model. Ecol. Appl. 1, 399–429.

Reichstein, M., Falge, E., Baldocchi, D., Papale, D., Aubinet, M., Berbigier, P., Bernhofer, C., Buchmann, N., Gilmanov, T., Granier, A., 2005. On the separation of net ecosystem exchange into assimilation and ecosystem respiration: review and improved algorithm. Global Change Biol. 11, 1424–1439.

Ruimy, A., Saugier, B., Dedieu, G., 1994. Methodology for the estimation of terrestrial net primary production from remotely sensed data. J. Geophys. Res. D: Atmos. 99, 5263–5283.

Running, S.W., Baldocchi, D.D., Turner, D.P., Gower, S.T., Bakwin, P.S., Hibbard, K.A., 1999a. A global terrestrial monitoring network integrating tower fluxes, flask sampling, ecosystem modeling and EOS satellite data. Remote Sens. Environ. 70, 108–127.

Running, S.W., Nemani, R., Glassy, J.M., Thornton, P.E., 1999b. MODIS Daily Photosynthesis (PSN) and Annual Net Primary Production (NPP) Product (MOD17) Algorithm Theoretical Basis Document. University of Montana, SCF At-Launch Algorithm ATBD Documents www.ntsg.umt.edu/modis/ATBD/ATBD_MOD17_v21.pdf.

Running, S.W., Nemani, R.R., Heinsch, F.A., Zhao, M., Reeves, M., Hashimoto, H., 2004. A continuous satellite-derived measure of global terrestrial primary production. Bioscience 54, 547–560.

Scott Green, D., Erickson, J.E., Kruger, E.L., 2003. Foliar morphology and canopy nitrogen as predictors of light-use efficiency in terrestrial vegetation. Agric. Forest Meteorol. 115, 163–171.

Stockli, R., Lawrence, D.M., Niu, G.Y., Oleson, K.W., Thornton, P.E., Yang, Z.L., Bonan, G.B., Denning, A.S., Running, S.W., 2008. Use of FLUXNET in the community land model development. J. Geophys. Res. G: Biogeosci. 113, G01025.

Suyker, A.E., Verma, S.B., Burba, G.G., Arkebauer, T.J., 2005. Gross primary production and ecosystem respiration of irrigated maize and irrigated soybean during a growing season. Agric. Forest Meteorol. 131, 180–190.

Tucker, C.J., 1979. Red and photographic infrared linear combinations for monitoring vegetation. Remote Sens. Environ. 8, 127–150.

Turner, D.P., Ritts, W.D., Cohen, W.B., Gower, S.T., Running, S.W., Zhao, M., Costa, M.H., Kirschbaum, A.A., Ham, J.M., Saleska, S.R., 2006. Evaluation of MODIS NPP and GPP products across multiple biomes. Remote Sens. Environ. 102, 282–292.

Turner, D.P., Ritts, W.D., Cohen, W.B., Gower, S.T., Zhao, M., Running, S.W., Wofsy, S.C., Urbanski, S., Dunn, A.L., Munger, J.W., 2003. Scaling gross primary production (GPP) over boreal and deciduous forest landscapes in support of MODIS GPP product validation. Remote Sens. Environ. 88, 256–270.

Turner, D.P., Ritts, W.D., Cohen, W.B., Maeirsperger, T.K., Gower, S.T., Kirschbaum, A.A., Running, S.W., Zhao, M., Wofsy, S.C., Dunn, A.L., 2005. Site-level evaluation of satellite-based global terrestrial gross primary production and net primary production monitoring. Global Change Biol. 11, 666–684.

Wagle, P., Kakani, V.G., 2014a. Environmental control of daytime net ecosystem exchange of carbon dioxide in switchgrass. Agric. Ecosyst. Environ. 186, 170–177.

Wagle, P., Kakani, V.G., 2014b. Seasonal variability in net ecosystem carbon dioxide exchange over a young switchgrass stand. GCB Bioenerg. 6, 339–350.

Wagle, P., Xiao, X., Torn, M.S., Cook, D.R., Matamala, R., Fischer, M.L., Jin, C., Dong, J., Biradar, C., 2014. Sensitivity of vegetation indices and gross primary production of tallgrass prairie to severe drought. Remote Sens. Environ. 152, 1–14.

Williams, M., Richardson, A.D., Reichstein, M., Stoy, P.C., Peylin, P., Verbeeck, H., Carvalhais, N., Jung, M., Hollinger, D.Y., Kattge, J., Leuning, R., Luo, Y., Tomelleri, E., Trudinger, C.M., Wang, Y.P., 2009. Improving land surface models with FLUXNET data. Biogeosciences 6, 1341–1359.

Winjum, J.K., Dixon, R.K., Schroeder, P.E., 1992. Estimating the global potential of forest and agroforest management practices to sequester carbon. Water Air Soil Poll. 64, 213–227.

Xiao, X., Hollinger, D., Aber, J., Goltz, M., Davidson, E.A., Zhang, Q., Moore III, B., 2004a. Satellite-based modeling of gross primary production in an evergreen needleleaf forest. Remote Sens. Environ. 89, 519–534.

Xiao, X., Zhang, Q., Braswell, B., Urbanski, S., Boles, S., Wofsy, S., Moore III, B., Ojima, D., 2004b. Modeling gross primary production of temperate deciduous broadleaf forest using satellite images and climate data. Remote Sens. Environ. 91, 256–270.

Yan, H.M., Fu, Y.L., Xiao, X.M., Huang, H.Q., He, H.L., Ediger, L., 2009. Modeling gross primary productivity for winter wheat–maize double cropping system using MODIS time series and CO_2 eddy flux tower data. Agric. Ecosyst. Environ. 129, 391–400.

Yilmaz, M.T., Hunt Jr., E.R., Jackson, T.J., 2008. Remote sensing of vegetation water content from equivalent water thickness using satellite imagery. Remote Sens. Environ. 112, 2514–2522.